Marginal reefs under stress: physiological limits render Galápagos corals susceptible to ocean acidification and thermal stress

Short title: Physiological limits to corals' buffering capacity

Diane Thompson,[1*] Malcolm McCulloch,[2] Julia E. Cole,[3] Emma V. Reed,[1] Juan P. D'Olivo,[4] Kelsey Dyez,[3] Marcus Lofverstrom,[1] Janice Lough,[5,6] Neal Cantin,[5] Alexander W. Tudhope,[7] Anson H. Cheung,[8] Lael Vetter,[1] R. Lawrence Edwards[9]

[1]University of Arizona, Department of Geosciences, Tucson, 85721, USA
[2]University of Western Australia, ARC Centre of Excellence for Coral Reefs Studies,Oceans Graduate School and Oceans Institute, Crawley, 6009, Australia
[3]University of Michigan, Earth and Environmental Sciences, Ann Arbor, 48109, USA
[4]Freie Universität Berlin, Berlin, 12249, Germany
[5]Australian Institute of Marine Science, PMB 3, Townsville MC, Queensland 4810, Australia
[6]ARC Centre of Excellence for Coral Reef Studies, James Cook University, Townsville, Queensland 4811, Australia
[7]University of Edinburgh, School of Geosciences, Edinburgh EH9 3JW, U.K.
[8]Department of Earth, Environmental, and Planetary Sciences, Brown University, Providence, RI 02912
[9]Department of Earth Sciences, University of Minnesota, Minneapolis, MN

Supplementary materials

Supplementary Text
Figs. S-1 to S-10
Tables S-1 to S-9

Implications for coral paleoclimate records

Because photosynthesis-mediated active transport (via Ca-ATPase or other alkalinity pumps) is critical for regulating the geochemistry of the calcifying fluid (as reviewed by Thompson, 2021), the changes reported here are likely to impact coral trace elemental (TE) proxy records (e.g., the commonly utilized Sr/Ca and Li/Mg paleothermometers), though the impact is likely to vary among colonies with differing susceptibility to stress (Cheung et al., 2021). A reduction in calcification rate or calcification efficiency alone would be expected to *decrease* the impact of Rayleigh fractionation on trace elemental ratios, while a reduction in active (energy intensive) Ca-ATPase transport would be expected to decrease the rate at which this isolated calcifying fluid is "refreshed" (relying more heavily on passive transport of ions) and thus *increase* the impact of Rayleigh fractionation across a range of calcification rates for elements that are discriminated against by the Ca-ATPase pump. For example, the coral Ca-ATPase pump displays little discrimination between Sr^{2+} and Ca^{2+} (with a transport stoichiometry Sr:Ca of 0.97, Marchitto et al., 2018); therefore, the Sr/Ca_{cf} is largely independent of the relative role of active vs. passive transport, and the calcification term likely dominates Rayleigh fractionation. Comparison of among TE/Ca proxies deferentially impacted by Rayleigh fractionation and the Ca-ATPase pump may therefore provide insight into the impact of thermal stress and ocean acidification on commonly utilized geochemical proxies for paleoclimate reconstructions (e.g., Cheung et al., 2021).

Corresponding author: Diane M. Thompson, `thompsod@arizona.edu`

Variations in growth parameters through time are likely to impact the fidelity of geochemical proxies from the Galápagos during thermal extremes (Cheung et al., 2021), as found at other sites (D'Olivo & McCulloch, 2017; D'Olivo et al., 2019; Clarke et al., 2019). Across the longest core (GW10-10), mean calcification dropped by 6% (0.152 g cm^{-2} yr^{-1}) between the WLF10-10c and WLF10-10a sections (i.e., following both the 1982/83 and 1997/98 thermal stress events), though this is within the range of interannual growth variations at this site (15-27%, Fig. S7, Table S6). Both WLF10-03 and WLF10-10a also displayed calcification anomalies (of 37 and 14%, respectively) during the 1997/98 event.

To assess the impact of these changes on Rayleigh fractionation, we regress Sr/Ca (thought to be influenced by temperature and Rayleigh fractionation) against Mg/Ca and U/Ca (Fig. S1f-g, assumed to be dictated by Rayleigh fraction, with little-to-no temperature effect). Although Mg/Ca and U/Ca may at times covary with SST, our new understanding of biomineralization strongly suggests that the apparent SST relationships with these elements are incidental to their control by Rayleigh fractionation (Reynaud et al., 2007; DeCarlo et al., 2015). Consistent with previous work, we find a strong negative relationship between Mg/Ca and Sr/Ca, and a strong positive relationship between U/Ca and Sr/Ca, in both modern and fossil Galápagos corals. In both cases, the (negative Mg/Ca-Sr/Ca, positive U/Ca-Sr/Ca) relationship weakens after the 1997/1998 thermal stress event (Fig. S6g-h), and the relationship between Mg/Ca and Sr/Ca also weakens between fossil and modern corals (Fig. 2f, explaining 68% and 14% of the variance, respectively). Finally, the difference in the slope of the pH_{cf}-SST relationship reconstructed from Sr/Ca and Li/Mg was also more pronounced in the fossil coral (compared to the modern corals), consistent with greater Rayleigh fractionation and thus larger offsets between these the paleothermometers in the fossil coral (Fig. S8). Assessing other trace elemental ratios prior to and following the 1997/1998 stress event, we find significant changes among geochemical parameters that are most sensitive to changes in Ca-ATPase pump activity, [CO_3^-], and Rayleigh fractionation (e.g., U/Ca, Mg/Ca, $\delta^{13}C$), and a weak (not statistically significant) change in those that are sensitive to Rayleigh fractionation and/or DIC_{cf} alone (e.g., Sr/Ca, B/Ca, pH_{cf}, Ω_{cf}). Critically, we also find a significant change in the Li/Mg–Sr/Ca relationship post 97/98 (Fig. S6i), suggesting that residual non-climate impacts may remain in the Li/Mg proxy. This breakdown in the Li/Mg–Sr/Ca relationship following following thermal stress has been observed at other sites (D'Olivo et al., 2019; Clarke et al., 2019), and could be related to changes in density banding and biosmoothing (Clarke et al., 2019); future studies across additional sites and extreme events are required to further explore these mechanisms. Taken together, our results indicate that although Galápagos modern corals may be less susceptible to the impacts of Rayleigh fractionation (particularly following thermal stress), other elemental ratios are strongly impacted by the reduction in Ca-ATPase efficiency (see also Cheung et al., 2021). Therefore, additional experimental work is critically needed to constrain the estimates of K_D (which dictates the impact of Rayleigh fractionation) and the transport stoichiometry of the Ca-ATPase pump across a variety of paleo-climate relevant trace elements.

Nevertheless, we demonstrate that our findings are robust to the paleo-thermometer used to assess the impact of temperature on coral carbonate chemistry. For example, across all methods used to reconstruct SST, pH_{cf} displays a strong negative relationship with temperature, and this relationship weakens considerably between fossil and modern corals. The slope and strength of this relationship is nearly identical for Li/Mg-SST and Sr/Ca-SST reconstructions (m_{fossil} = -0.031 vs. -0.024; r^2_{fossil} = 0.4 vs. 0.37; m_{modern} = -0.012 vs -0.01; r^2_{modern} = 0.27 vs 0.24; Fig. S8). However, all three paleo-thermometers overestimate the strength of the relationship in modern corals (for which observed SSTs are available for comparison). Therefore, the breakdown of pH upregulation in modern corals may be even worse than predicted by the proxy records.

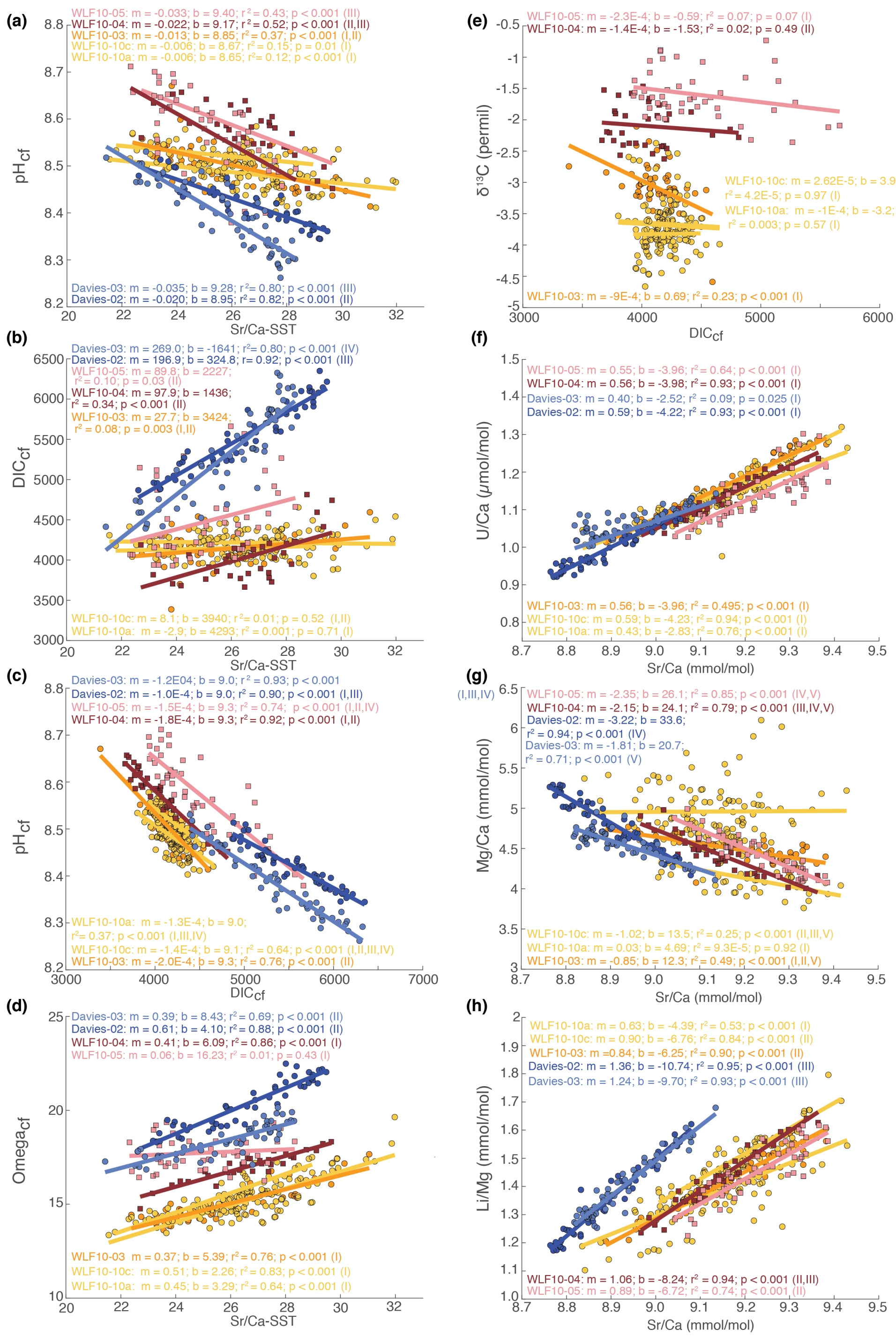

Figure S-1. Comparison of the relationships among geochemical proxies, by core: Galápagos 18th-century fossil (red & pink squares) and modern (20th century, orange & yellow circles) versus Great Barrier Reef modern (blue circles). (a) Sr/Ca-SST vs. pH_{cf}, (b) Sr/Ca-SST vs. DIC_{cf}, (c) pH_{cf} vs. DIC_{cf}, (d) Sr/Ca-SST vs. Ω_{cf}, (e) DIC_{cf} vs. $\delta^{13}C$, (f) Sr/Ca vs. U/Ca, (g) Sr/Ca vs. Mg/Ca, and (h) Sr/Ca vs. Li/Mg

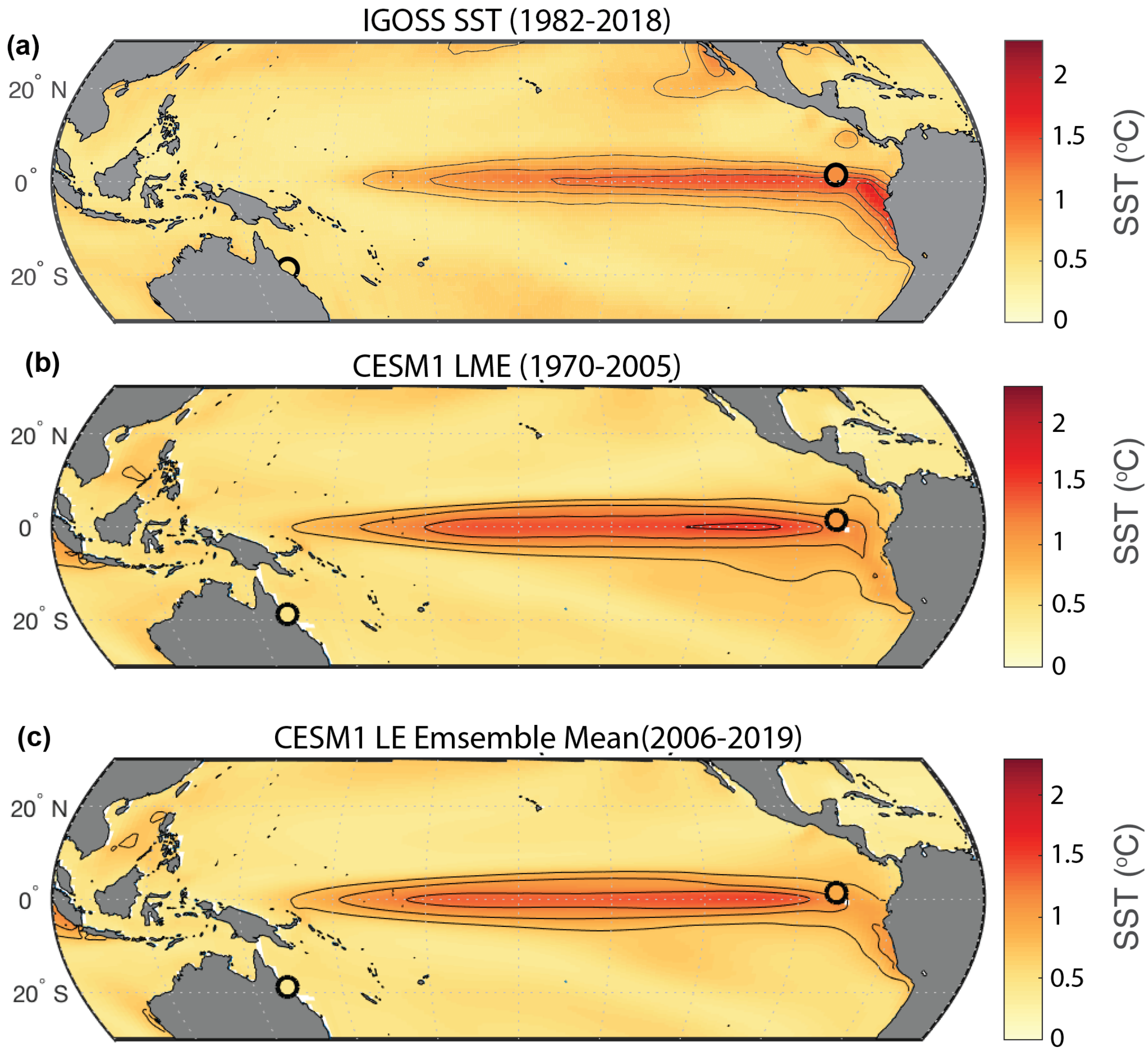

Figure S-2. Comparison of interannual SST anomalies: satellite (IGOSS), CESM1 LME, and CESM1 LE. Standard deviation of monthly sea surface SST anomalies (a) CESM1 LME over the 1970-2005 climatolgical period used in this study, (b) IGOSS SST over the 1982-2018 period of coverage, (c) CESM1 LE ensemble mean over the 2006-2019 baseline period used in this study.

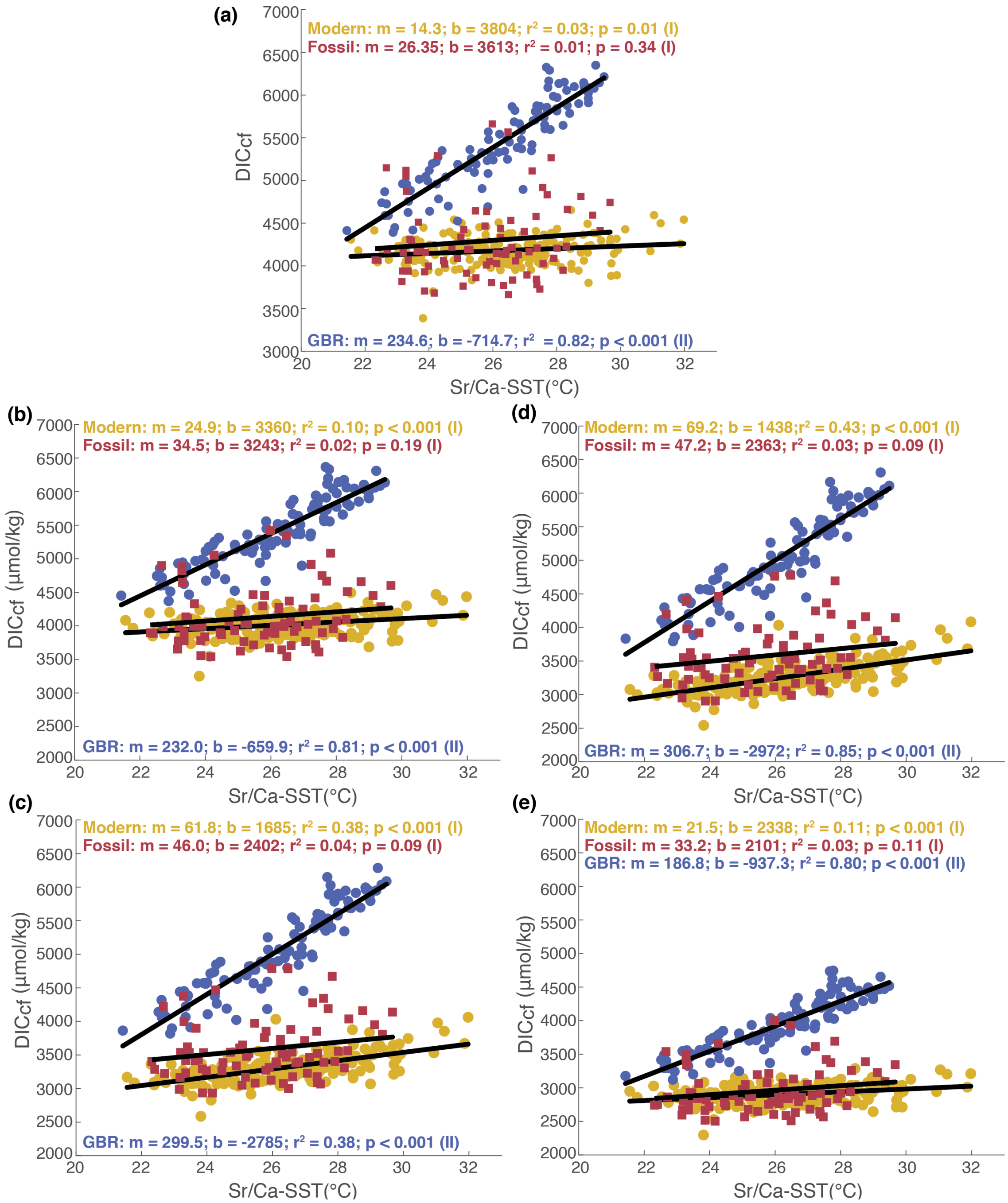

Figure S-3. Comparison of the Sr/Ca-SST vs. DIC_{cf} relationship among geochemical proxies, Wolf 18th-century fossil (red squares) and modern (20th century, orange circles) versus Great Barrier Reef modern (blue circles). Top panel as in Figure 3e, along with other formulations of K_D: (a) McCulloch et al. (2017) refit by DeCarlo et al. 2018, (b) DeCarlo et al. 2018, (c) Holcomb et al. (2016) equation 7, and (d) constant of 0.002 (after Allison, 2017). In all panels, roman numerals (I-III) denote relationships that are significantly different from other groups, based on ANCOVA and multiple comparisons (where a significant difference among groups was identified). Groups with the same roman numeral are not significantly different from one another.

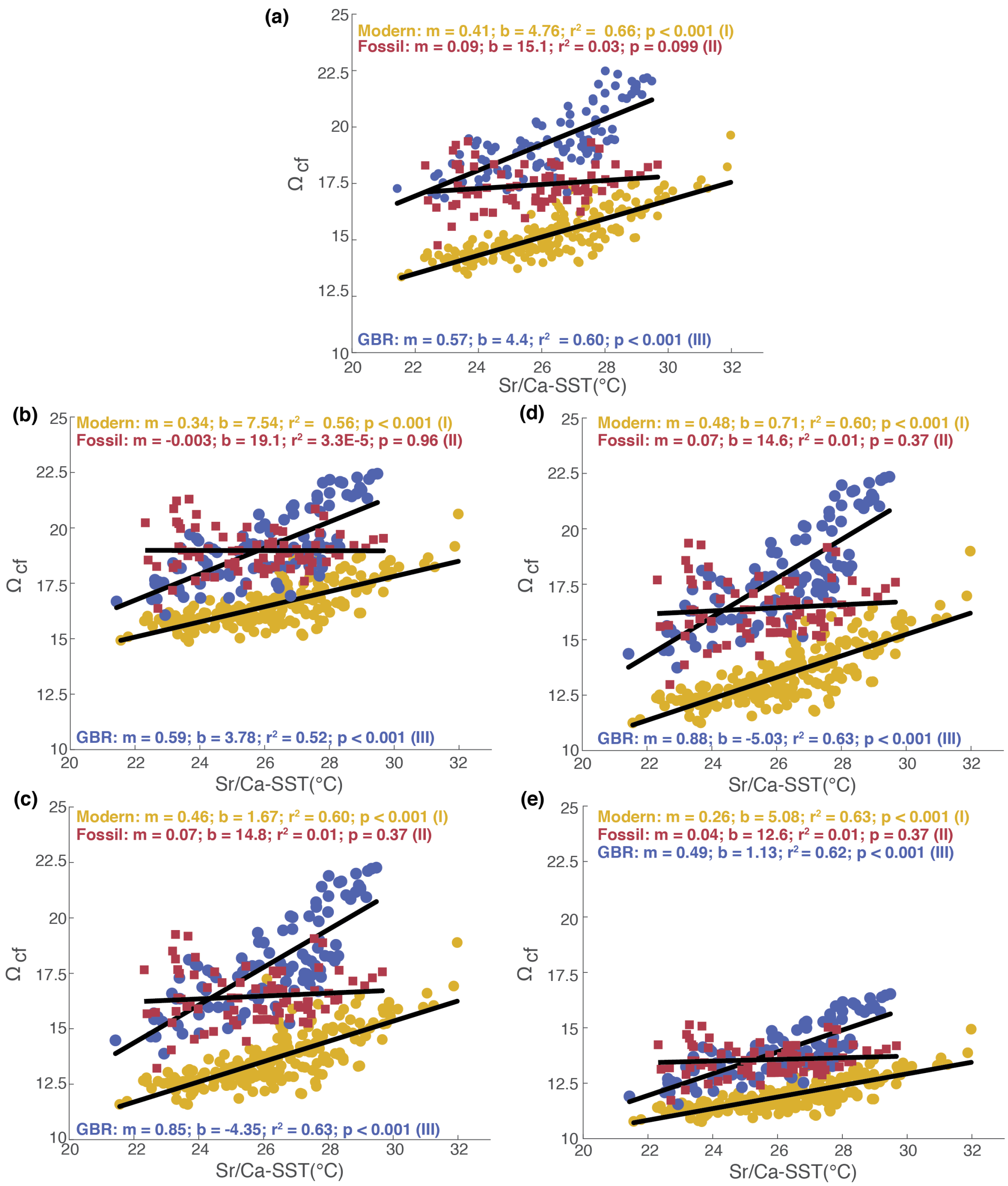

Figure S-4. Comparison of the Sr/Ca-SST vs. Ω_{cf} relationship among geochemical proxies, Wolf 18th-century fossil (red squares) and modern (20th century, orange circles) versus Great Barrier Reef modern (blue circles). Top panel as in Figure 3e, along with other formulations of KD: (a) McCulloch et al. (2017) refit by DeCarlo et al. 2018, (b) DeCarlo et al. 2018, (c) Holcomb et al. (2016) equation 7, and (d) constant of 0.002 (after Allison, 2017). In all panels, roman numerals (I-III) denote relationships that are significantly different from other groups, based on ANCOVA and multiple comparisons (where a significant difference among groups was identified). Groups with the same roman numeral are not significantly different from one another.

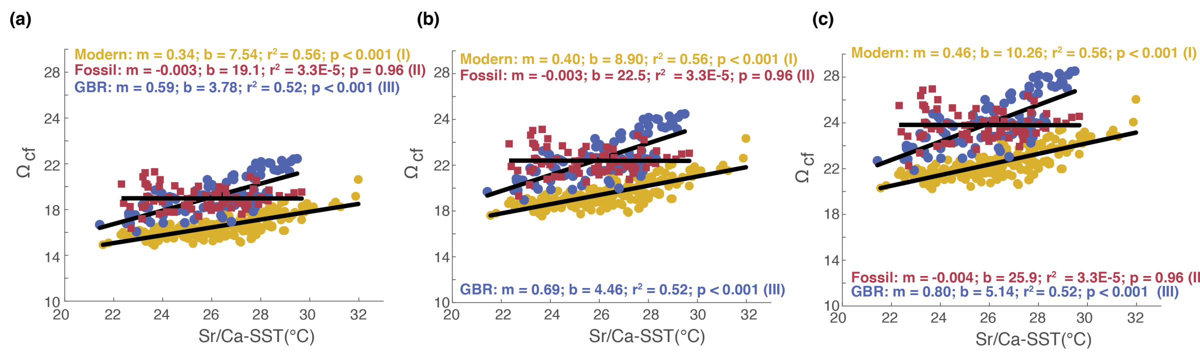

Figure S-5. Comparison of the Sr/Ca-SST vs. Ω_{cf} relationship among geochemical proxies, Wolf 18th-century fossil (red squares) and modern (20th century, orange circles) versus Great Barrier Reef modern (blue circles). Sensitivity test of the upregulation of $[Ca^{2+}]$ relative to seawater: (a) as in Figure 3e ($[Ca^{2+}]$ scaling factor = 1; -1SD from Sevilgen et al. 2019), (b) $[Ca^{2+}]$ scaling factor = 1.18 (mean value from Sevilgen et al. 2019), (c) $[Ca^{2+}]$ scaling factor = 1.36 (+1SD from Sevilgen et al. 2019). In all panels, roman numerals (I-III) denote relationships that are significantly different from other groups, based on ANCOVA and multiple comparisons (where a significant difference among groups was identified). Groups with the same roman numeral are not significantly different from one another.

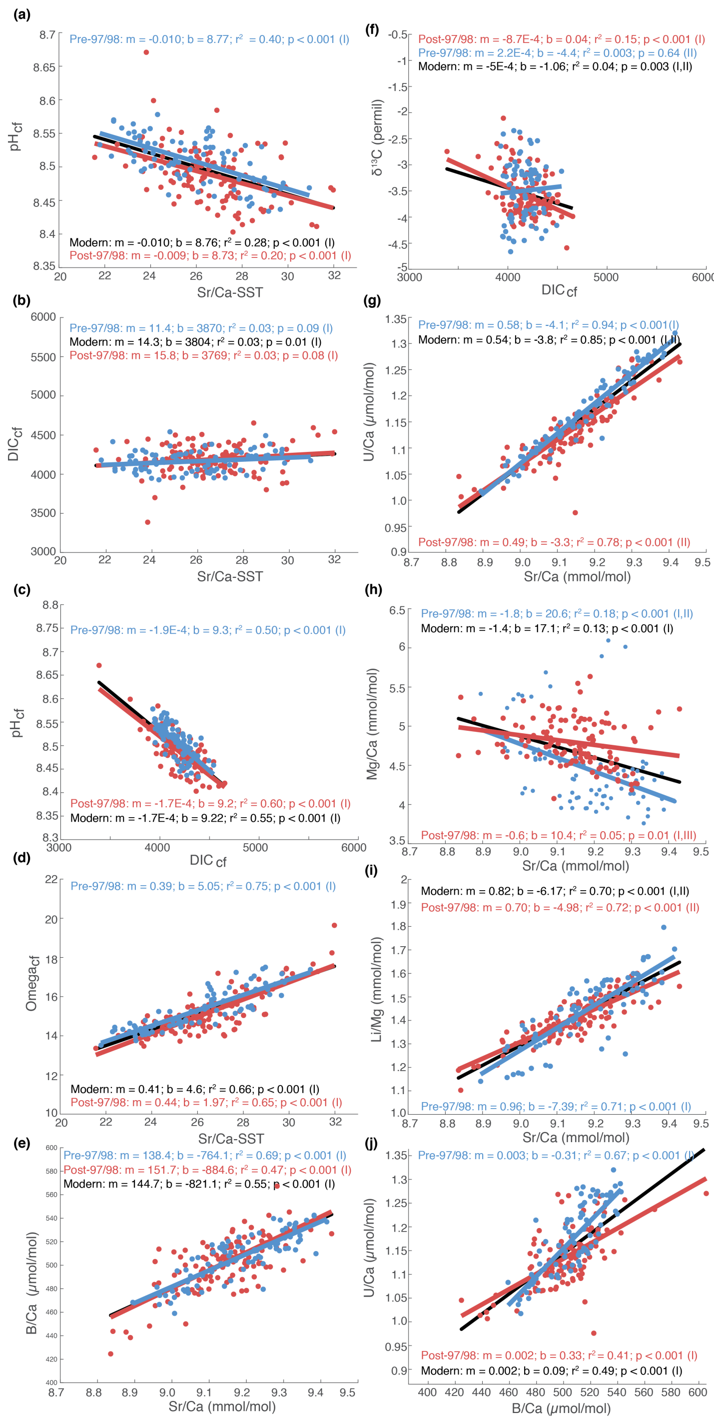

Figure S-6. Comparison of pre- and post-bleaching relationships: (a) Sr/Ca-SSTs vs. pH_{cf}, (b) Sr/Ca-SSTs vs. DIC_{cf}, (c) Sr/Ca-SSTs vs. Ω_{cf}, and (d) Sr/Ca vs. Mg/Ca for all modern coral data (black), pre- 1997/1998 thermal stress (blue), and post- 1997/1998 thermal stress (red).

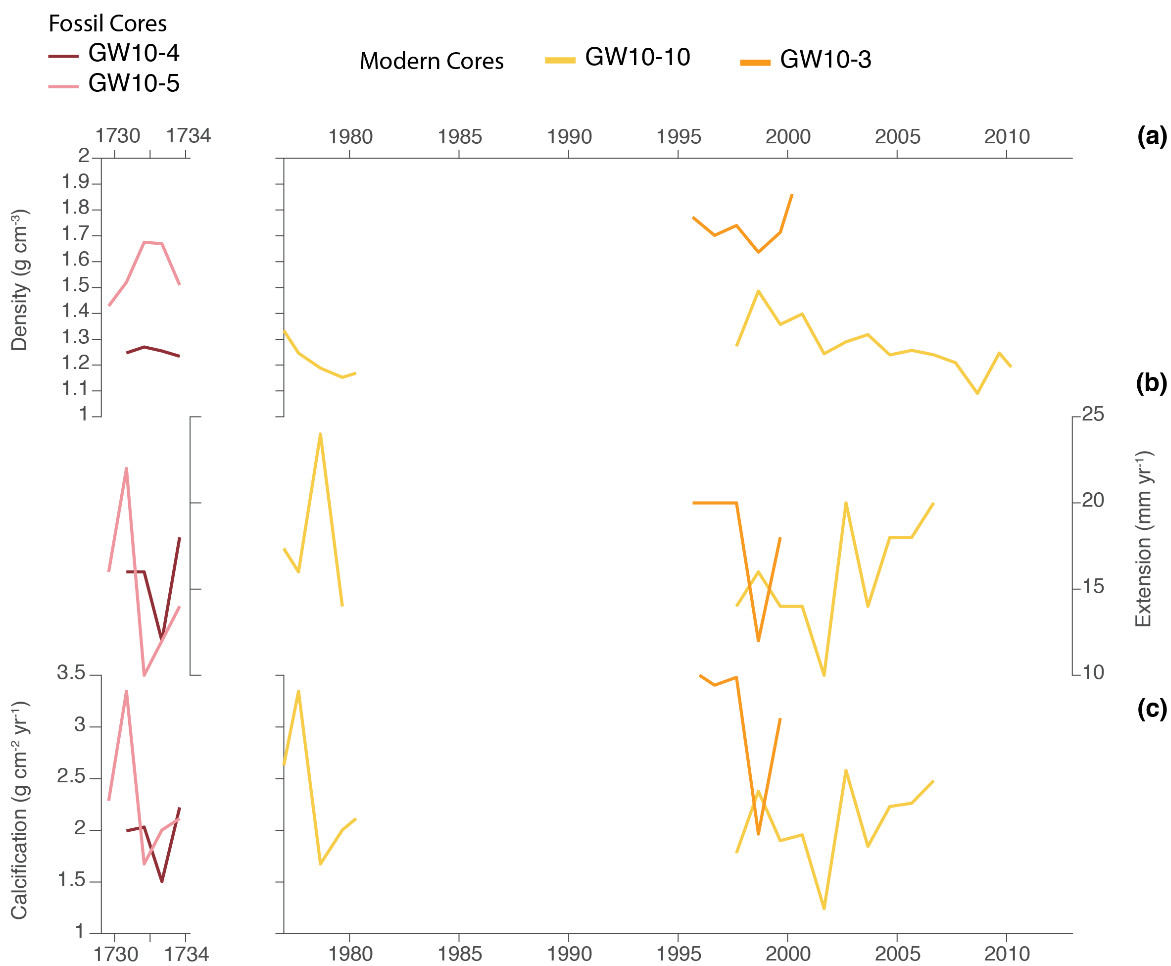

Figure S-7. **Coral growth timeseries**: (a) average annual skeletal density (g cm^{-3}), (b) linear extension (cm yr^{-1}), and (c) calcification (g cm^{-2} yr^{-1}) for all cores analyzed in this study. Skeletal density was calculated across 2 transects on either side of the geochemical sampling transect (T1 & T2) from which the average density was calculated to account for variations associated with skeletal architecture and other within slab variations.

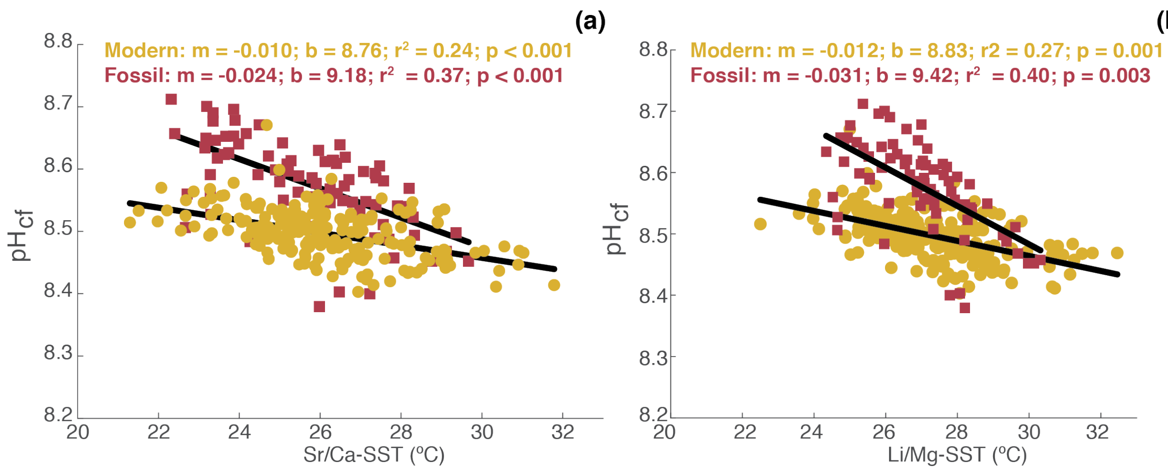

Figure S-8. Sensitivity of pH$_{sw}$ vs. SST to reconstruction: (a) Sr/Ca-SST and (b) Li/Mg-SST.

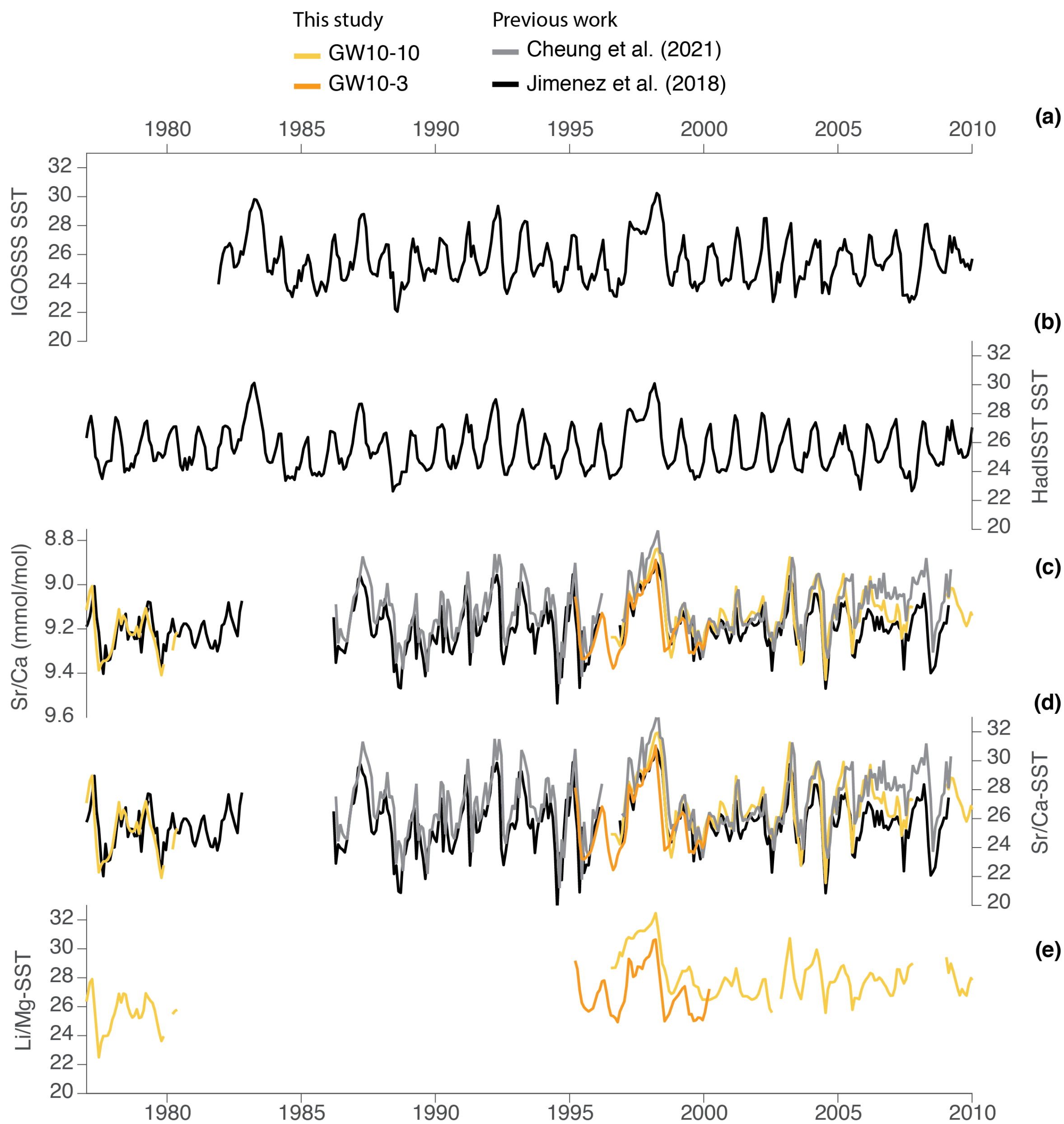

Figure S-9. Time series of: (a) IGOSS SST (°C), (b) HadISST SST (°C), (c) Sr/Ca (mmol/mol), (d) Sr/Ca-SST (°C), (e) Li/Mg-SST (°C) for WLF modern (GW10-10, yellow; GW10-3) cores analyzed in this study. Sr/Ca (a) measured at the University of Arizona (Jimenez et al., 2018; Cheung et al., 2021) is shown for comparison.

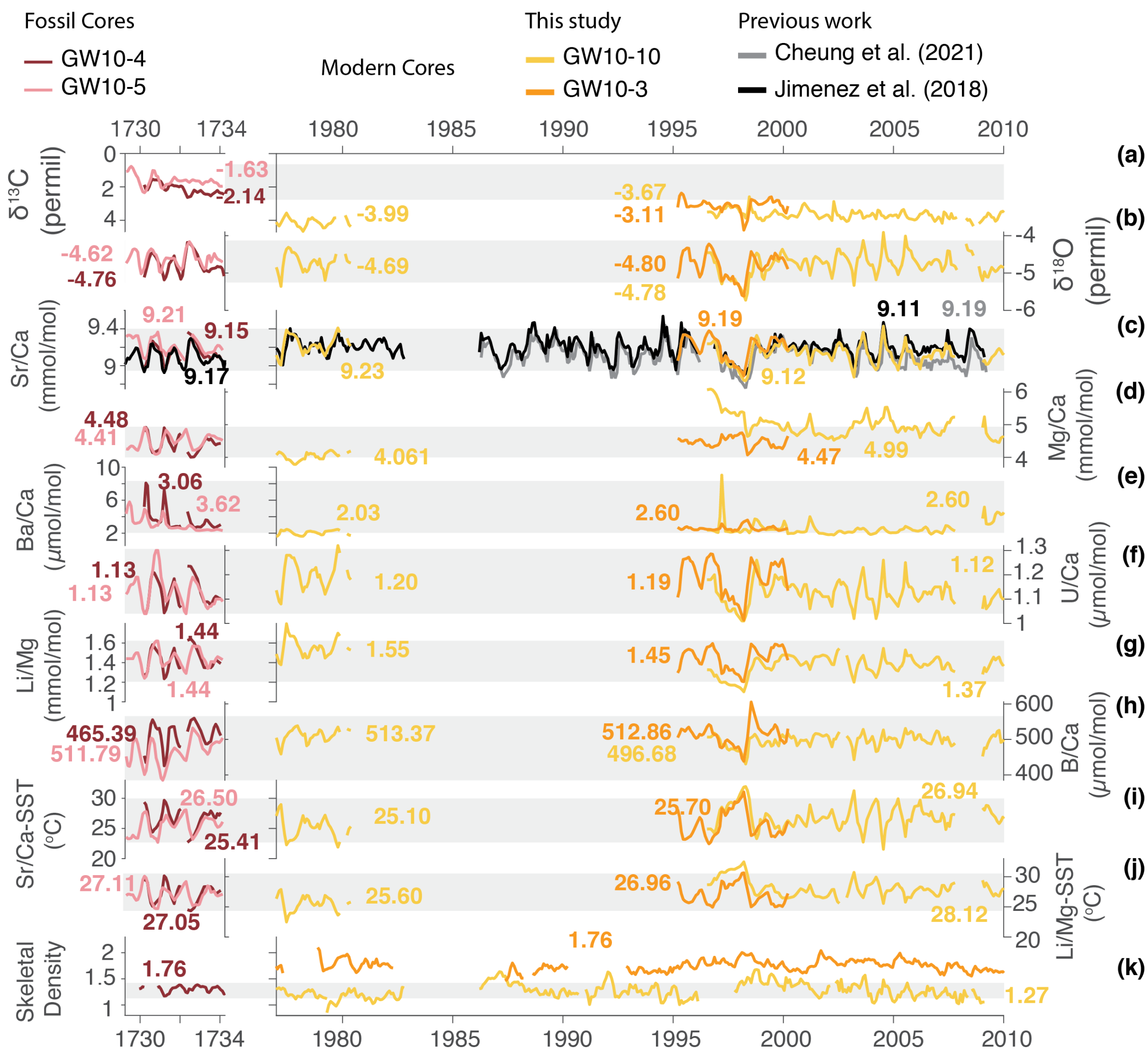

Figure S-10. **Time series of:** (a) δ^{13}C (permil), (b) δ^{18}O (permil), (c) Sr/Ca (mmol/mol), (d) Mg/Ca (mmol/mol), (e) Ba/Ca (mmol/mol), (f) U/Ca (μmol/mol), (g) Li/Mg (mmol/mol), (h) B/Ca (μmol/mol), (i) Sr/Ca-SST (°C), (j) Li/Mg-SST (°C), and (k) skeletal density (g/cm^3) for WLF fossil (GW10-4, red; GW10-5, pink) and modern (GW10-10, yellow; GW10-3) cores analyzed in this study. Sr/Ca (a) measured at the University of Arizona (Jimenez et al., 2018; Cheung et al., 2021) is shown for comparison. Gray bars indicate the range of fossil values.

Table S-1. Geochemical "proxies" utilized in this study. The primary, reconstructed parameter and other secondary factors driving variability in each proxy measurement are listed. Interpretation here represents the current understanding of these geochemical proxies in the coral paleoclimate community, and may change as our understanding of biomineralization continues to evolve with studies such as this one.

Measured geochemical "proxy"	Primary (reconstructed) parameter	Secondary factors
Sr/Ca	SST	Rayleigh
B/Ca (+ δ^{11}B)	$[CO_3^-]_{cf}$	DIC_{cf}
Ba/Ca	Upwelling	
U/Ca	$[CO_3^-]_{cf}$	Rayleigh
Mg/Ca	Rayleigh	
Li/Ca	Temperature	Rayleigh
Li/Mg	Temperature	
δ^{11}B	pH_{cf}	
δ^{18}O	Temperature	Salinity
δ^{13}C	DIC source	

Table S-2. **Statistics of coral calcifying fluid (this study) and seawater geochemistry** (McCulloch et al., 2017; Humphreys et al., 2018) at the Galápagos and GBR study sites: mean (seasonal range, warm-cold).

	Calcifying fluid			Seawater		
	pH	**DIC**	Ω	**pH**	**DIC**	Ω
Great Barrier Reef				8.04 (-0.02)	1966.98 (-6.95)	3.50 (0.07)
Davies 13-02	8.42 (-0.03)	5549.33 (311.6)	20.30 (1.13)			
Davies 13-03	8.39 (-0.05)	5317.86 (423.9)	18.42 (0.82)			
Galápagos modern				8.07 (N/A)	N/A	3.20 (N/A)
WLF10-03	8.51 (-0.003)	4142.88 (0.91)	15.02 (0.38)			
WLF10-10a	8.48 (-0.01)	4212.54 (20.0)	15.38 (0.57)			
WLF10-10c	8.52 (-0.02)	4149.18 (78.6)	15.08 (0.78)			
Galápagos fossil				N/A	N/A	N/A
WLF10-04	8.58 (-0.05)	4023.66 (306.2)	17.61 (0.19)			
WLF10-05	8.57 (-0.06)	4523.73 (288.0)	17.00 (0.27)			

Table S-3. Validation of CESM1 carbonate system: comparison of pH, dissolved inorganic carbon (DIC) and aragonite saturation (Ω) at the Great Barrier Reef (GBR) and Galápagos coral sites analyzed in this study. Values are shown for in situ observations (McCulloch et al., 2017; Humphreys et al., 2018), GLODAPv2 climatology (1972-2013), CESM1 LME climatology (1970-2005) and CESM1 LE climatology (2006-2013). CESM1 LE multi-ensemble member mean (N=34), ensemble maximum, and ensemble minimum are shown as an estimate of internal variability.

	Great Barrier Reef			**Galápagos**		
	pH	**DIC**	Ω	**pH**	**DIC**	Ω
in Situ Observations	8.0419	1967	3.4920	8.07	N/A	3.2
GLODAPv2 (1972-2013)	8.1105 (0.0294)	N/A	3.9372 (0.6104)	8.0473 (0.0091)	N/A	3.3208 (0.2075)
CESM1 LME (1970-2005)	8.1023	1898.6	3.726	8.0642	1917.5	3.3836
CESM1 LE (2006-2013)						
Ensemble mean (N=34)	8.0719	1910.4	3.5052	7.9759	1950.1	2.857
Ensemble maximum	8.0742	1919.7	3.5279	7.9820	1958.7	2.9146
Ensemble minimum	8.0701	1901.1	3.4704	7.9672	1942.7	2.7886
RSD (%)	0.3	1.5	5.1	0.6	N/A	8.3

Table S-4. **Pchange statistics**: Statistics for the percent upregulation of pH, DIC, and Ω within the coral calcifying fluid among *Porites* spp. colonies from: "all Galápagos" (N=385; 5 cores: this study); "Davies, GBR" (N=104; 2 cores: (McCulloch et al., 2017)); "Mesoamerican seeps" (N=98; 12 sites; (Wall et al., 2019)); and "Papua New Guinea (PNG) seeps" (N=14; 4 sites; (Wall et al., 2016)).

Site	Mean (Std)	Regress with Ω_{sw}			
		slope	b	r^2	p
pH Pchange					
All Galápagos	5.30 (0.66)	-0.8	8.1	0.73	0.02
Davies, GBR	4.12 (0.78)	N/A	N/A	N/A	N/A
Mesoamerica seeps	12.93 (2.6)	-2.8	17.2	0.91	$<$0.001
PNG seeps	4.71 (2.7)	-2.0	9.6	0.99	$<$0.01
DIC Pchange					
All Galápagos	117.0 (15.1)	17.1	50.9	0.19	0.46
Davies, GBR	184.4 (26.8)	N/A	N/A	N/A	N/A
Mesoamerica seeps	23.3 (30.7)	17.3	-2.4	0.43	0.02
PNG seeps	N/A	N/A	N/A	N/A	N/A
Ω Pchange					
All Galápagos	342.5 (31.7)	-11.8	364.6	0.02	0.81
Davies, GBR	451.0 (41.7)	N/A	N/A	N/A	N/A
Mesoamerica seeps	915.2(436.8)	-270.0	1354.3	0.75	$<$0.001
PNG seeps	494.7(292.3)	-214.3	1008.3	0.96	0.02

Table S-5. Regression of percent pH, DIC, and Ω upregulation (PChange, %) with Sr/Ca-SSTs. Values in italics, bold, and bold italics are significant at the 95, 99, and 99.9% confidence level, respectively.

	pH PChange			**DIC Pchange**			**Ω Pchange**		
	m	**b**	**r^2**	**m**	**b**	**r^2**	**m**	**b**	**r^2**
Great Barrier Reef	***-0.31***	***12.2***	***0.61***	***12.3***	***-137***	***0.82***	***16.3***	***25.3***	***0.59***
Davies 13-02	***-0.25***	***11***	***0.82***	***10.3***	***-83***	***0.92***	***17.4***	***16.8***	***0.88***
Davies 13-03	***-0.43***	***15***	***0.8***	***14.1***	***-186***	***0.8***	***11***	***140***	***0.69***
Galápagos modern	***-0.06***	***6.9***	***0.08***	*0.63*	*97.1*	*0.02*	***15.7***	***-78.4***	***0.69***
WLF10-03	***-0.17***	***9.6***	***0.36***	**1.7**	**65.9**	**0.11**	***10.5***	***40.3***	***0.77***
WLF10-10a	***-0.07***	***7.2***	***0.12***	-0.22	121.3	0.004	***13.9***	***-16.9***	***0.7***
WLF10-10c	***-0.08***	***7.1***	***0.21***	0.35	105.6	0.006	***12.3***	***-14***	***0.84***
Galápagos fossil	***-0.25***	***11.4***	***0.3***	1	99.7	0.01	**3.3**	**230.7**	**0.08**
WLF10-04	***-0.27***	***12.2***	***0.54***	***5.2***	***-27.9***	***0.37***	***9.9***	***43.4***	***0.87***
WLF10-5	***-0.36***	***13.8***	***0.38***	3.3	53.5	0.05	1.3	288.6	0.01

Table S-6. Coral growth statistics: average annual skeletal density (g cm^{-3}), linear extension (cm yr^{-1}), and calcification (g cm^{-2} yr^{-1}) for all cores analyzed in this study. Values in parenthesis denote the 1 sigma standard deviation. Skeletal density was calculated across 2 transects on either side of the geochemical sampling transect (T1 & T2) from which the average density was calculated to account for variations associated with skeletal architecture and other within slab variations.

Site	**Time**		**Density**		**Extension**	**Calcification**
		T1	T2	Avg		
All				1.39 (0.21)	1.64 (0.36)	2.29 (0.60)
Fossil				1.42 (0.18)	1.49 (0.41)	2.13 (0.52)
WLF04	1730 - 1733	1.25 (0.02)	1.29 (0.03)	1.25 (0.02)	1.55 (0.25)	1.94 (0.31)
WLF05	1729 - 1733	1.58 (0.12)	1.54 (0.11)	1.56 (0.11)	1.48 (0.46)	2.28 (0.63)
Modern				1.38 (0.23)	1.69 (0.34)	2.37 (0.64)
WLF10c	1976-1980	1.22 (0.08)	1.24 (0.11)	1.23 (0.09)	1.80 (0.43)	2.23 (0.54)
WLF10a	1997-2010	1.28 (0.11)	1.28 (0.09)	1.27 (0.10)	1.60 (0.31)	2.08 (0.38)
WLF03	1995-2000	1.8 (0.07)	1.66 (0.10)	1.74 (0.08)	1.80 (0.35)	3.10 (0.66)

Table S-7. Coral growth relationships: multivariate regression between average skeletal density (g cm^{-3}) and Ω_{cf} and Sr/Ca-SST for all cores analyzed in this study. Skeletal density was calculated across 2 transects on either side of the geochemical sampling transect (T1 & T2) from which the average density was calculated to account for variations associated with skeletal architecture and other within slab variations. The slope of the regression between annual skeletal density (g cm^{-3}) and annual linear extension (mm yr^{-1}) are also given for the entire core in Table S9 of (Reed et al., 2021). The inferred change in calcification rate (g cm^{-2} yr^{-1}) with warming and acidification (ΔG) is given for each core, based on the relationships among density and extension, temperature, and saturation.

Core	N	m, Omega	m, SST	b	r^2	p	m, Extension	Inferred deltaG
WLF-10a	157	0.028	-0.036	1.834	0.118	$<$0.001	1.7 (N=21)	**decreased**
WLF-10c	49	0.195	-0.065	-0.762	0.67	$<$0.001	1.7 (N=21)	**decreased**
WLF10 (a&c)	206	0.017	-0.0113	1.31	0.01	0.16	1.7 (N=21)	**decreased**
WLF-3	61	-0.075	0.026	2.18	0.207	$<$0.001	0.361 (N=52)	increased
WLF-4	49	0.018	-0.017	1.4	0.112	0.033	0.356 (N=77)	**decreased**
WLF-5	59	-0.091	0.012	2.85	0.42	$<$0.001	-3.2 (N=12)	**decreased**

Table S-8. Sensitivity and validation analysis for predicted Ω upregulation in GBR corals: in situ observations versus CESM1 LME and LE simulated monthly, seasonal average, and average Ω_{sw}. CESM1 LE (min, max and mean of the 34 ensemble members) compares well with in situ observations over the 2007-2013 and 2006-2013 periods of coverage for Davies 02 & 03, respectively. CESM1 LE was therefore used in this study for all records with coverage post-2005 (the end of CESM1 LME simulations). Similarly, the average Ω_{sw} value was used as a conservative estimate of the seasonal upregulation variability (shown in parentheses: warm minus cold season).

	Davies 02	Davies 03
In Situ Observations		
Monthly	481.8 (20.7)	426.4 (12.9)
Seasonal Avg.	482.2 (20.8)	426.6 (12.9)
Average	483.2 (32.3)	427.0 (23.4)
CESM1 LME		
Seasonal Avg. (1970-2005)	443.7 (18.4)	394.0 (11.2)
Average (1970-2005)	455.5 (30.8)	404.2 (22.4)
Predicted	501.3 (33.3)	444.8 (24.2)
CESM1 LE		
Min	477.2 (32.0)	422.7 (23.2)
Max	487.5 (32.6)	431.6 (23.6)
Mean	481.3 (32.0)	426.1 (23.4)

Table S-9. Validation analysis for predicted Ω upregulation in Galápagos corals: comparison of pH, DIC, and Ω upregulation (%, ± 1σ), using seawater values from (Humphreys et al., 2018) and CESM1 LME or LE over the interval of data coverage. Note that in situ observations reported by (Humphreys et al., 2018), were collected 3-8 June 2012 (Manzello et al., 2014)); these values are therefore not contemporaneous with any of the coral records studied here, and are likely to overestimate the amount of upregulation observed within the WLF modern records. The values for the youngest core (WLF10-10a, ending in 2010) are within 1σ error of one another (in situ vs. CESM1), giving us confidence in the CESM1-derived estimates (with reported conservative uncertainty of $\sim \pm 30\%$, which is within the 1σ range observed in individual cores).

	Time	**Humphreys et al. (2018)**			**CESM1 LME/LE**		
		pH	**DIC**	Ω	**pH**	**DIC**	Ω
Fossil							
WLF10-4	1730 - 1733	N/A	N/A	N/A	4.93 (0.65)	110.5 (14.9)	307.6 (18.6)
WLF10-5	1729 - 1733	N/A	N/A	N/A	4.69 (0.86)	136.6 (21.6)	322.6 (18.6)
Modern							
WLF10-10c	1976-1980	5.32 (0.38)	N/A	371.3 (28.2)	4.97 (0.32)	114.3 (7.6)	296.0 (23.7)
WLF10-10a	1997-2010	5.11 (0.36)	N/A	380.8 (31.9)	4.98 (0.36)	114.6 (6.7)	334.3 (28.8)
WLF10-03	1995-2000	5.27 (0.48)	N/A	368.0 (29.5)	5.18 (0.6)	109.8 (11.1)	311.1 (26.0)

References

Cheung, A. H., Cole, J. E., Thompson, D. M., Vetter, L., Jimenez, G., & Tudhope, A. W. (2021). Fidelity of the coral Sr/Ca paleothermometer following heat stress in the northern Galápagos. *Paleoceanography and Paleoclimatology*, e2021PA004323.

Clarke, H., D'Olivo, J., Conde, M., Evans, R., & McCulloch, M. (2019). Coral Records of Variable Stress Impacts and Possible Acclimatization to Recent Marine Heat Wave Events on the Northwest Shelf of Australia. *Paleoceanography and Paleoclimatology*, *34*(11), 1672–1688.

DeCarlo, T. M., Gaetani, G. A., Holcomb, M., & Cohen, A. L. (2015). Experimental determination of factors controlling U/Ca of aragonite precipitated from seawater: Implications for interpreting coral skeleton. *Geochimica et Cosmochimica Acta*, *162*, 151–165.

D'Olivo, J., & McCulloch, M. (2017). Response of coral calcification and calcifying fluid composition to thermally induced bleaching stress. *Scientific reports*, *7*(1), 1–15.

D'Olivo, J. P., Georgiou, L., Falter, J., DeCarlo, T. M., Irigoien, X., Voolstra, C. R., ... McCulloch, M. T. (2019). Long-term impacts of the 1997–1998 bleaching event on the growth and resilience of massive Porites corals from the central Red Sea. *Geochemistry, Geophysics, Geosystems*, *20*(6), 2936–2954.

Humphreys, A. F., Halfar, J., Ingle, J. C., Manzello, D., Reymond, C. E., Westphal, H., & Riegl, B. (2018). Effect of seawater temperature, pH, and nutrients on the distribution and character of low abundance shallow water benthic foraminifera in the Galápagos. *PloS one*, *13*(9).

Jimenez, G., Cole, J. E., Thompson, D. M., & Tudhope, A. W. (2018). Northern Galápagos corals reveal twentieth century warming in the eastern tropical Pacific. *Geophysical Research Letters*, *45*(4), 1981–1988.

Manzello, D. P., Enochs, I. C., Bruckner, A., Renaud, P. G., Kolodziej, G., Budd, D. A., ... Glynn, P. W. (2014). Galápagos coral reef persistence after ENSO warming across an acidification gradient. *Geophysical Research Letters*, *41*(24), 9001–9008.

Marchitto, T., Bryan, S., Doss, W., McCulloch, M., & Montagna, P. (2018). A simple biomineralization model to explain Li, Mg, and Sr incorporation into aragonitic foraminifera and corals. *Earth and Planetary Science Letters*, *481*, 20–29.

McCulloch, M. T., D'Olivo, J. P., Falter, J., Holcomb, M., & Trotter, J. A. (2017). Coral calcification in a changing world and the interactive dynamics of pH and DIC upregulation. *Nature communications*, *8*(1), 1–8.

Reed, E. V., Thompson, D. M., Cole, J. E., Lough, J. M., Cantin, N. E., Cheung, A. H., ... Edwards, R. L. (2021). Impacts of coral growth on geochemistry: Lessons from the galápagos islands. *Paleoceanography and Paleoclimatology*, *36*(4), e2020PA004051.

Reynaud, S., Ferrier-Pages, C., Meibom, A., Mostefaoui, S., Mortlock, R., Fairbanks, R., & Allemand, D. (2007). Light and temperature effects on Sr/Ca and Mg/Ca ratios in the scleractinian coral Acropora sp. *Geochimica et Cosmochimica Acta*, *71*(2), 354–362.

Thompson, D. M. (2021). Environmental records from coral skeletons: A decade of novel insights and innovation. *Wiley Interdisciplinary Reviews: Climate Change*, e745.

Wall, M., Fietzke, J., Crook, E., & Paytan, A. (2019). Using B isotopes and B/Ca in corals from low saturation springs to constrain calcification mechanisms. *Nature communications*, *10*(1), 1–9.

Wall, M., Fietzke, J., Schmidt, G. M., Fink, A., Hofmann, L., De Beer, D., & Fabricius, K. (2016). Internal pH regulation facilitates in situ long-term acclimation of massive corals to end-of-century carbon dioxide conditions. *Scientific reports*, *6*, 30688.